Cement and Concrete Research 42 (2012) 1001–1013

Contents lists available at SciVerse ScienceDirect

Cement and Concrete Research

journal homepage: http://ees.elsevier.com/CEMCON/default.asp

Water retention and gas relative permeability of two industrial concretes

Wei Chen [a,b,c], Jian Liu [a,b,c], Flore Brue [a,b,c], Frédéric Skoczylas [a,b,c], C.A. Davy [a,b,c,*], Xavier Bourbon [d], Jean Talandier [d]

[a] Univ Lille Nord de France, F-59000 Lille, France
[b] ECLille, LML, BP 48, F-59650 Villeneuve d'Ascq, France
[c] CNRS, UMR 8107, F-59650 Villeneuve d'Ascq, France
[d] Andra, 1–7 rue Jean Monnet, F-92298 Châtenay-Malabry Cedex, France

ARTICLE INFO

Article history:
Received 3 May 2011
Accepted 3 April 2012

Keywords:
Sorption/desorption (C)
Water retention (C)
Permeability (C)
Concrete (E)
Waste management (E)

ABSTRACT

This experimental study aims at identifying the water retention properties of two industrial concretes to be used for long term underground nuclear waste storage structures. Together with water retention, gas transfer properties are identified at varying water saturation level, i.e. relative gas permeability is assessed *directly* as a function of water saturation level S_w. The influence of the initial de-sorption path and of the subsequent re-saturation are analysed both in terms of water retention and gas transfer properties. Also, the influence of concrete microstructure upon water retention and relative gas permeability is assessed, using porosity measurements, analysis of the BET theory from water retention properties, and MIP. Finally, a single relative gas permeability curve is proposed for each concrete, based on Van Genuchten–Mualem's statistical model, to be used for continuous modelling approaches of concrete structures, both during drying and imbibition.

1. Introduction

The two concretes involved in this experimental study have been designed by the French National Agency for Nuclear Waste Management (Andra) as possible candidates for long-term repository. These concretes will be used for containers and/or for tunnels intended for the disposal of so-called HA and MAVL radioactive wastes (i.e. long or intermediate activity and long life radioactive nuclear wastes). Long-term disposal structures will be built into a clayey rock layer (argillite), currently under investigation in the East of France at Bure [1]. Located in an argillite layer at ca. −500 m depth, a dedicated laboratory has been designed to perform realistic in situ studies and to help evaluate the storage feasibility and safety over thousands of years. In particular, at the beginning of its life within the disposal structure, concrete will be submitted to increasing temperatures due to waste presence and to tunnel ventilation, leading to its drying. After sealing, the whole structure (i.e. tunnel and argillite in contact with concrete) will be progressively re-saturated with pore water coming back from the more distant rock, due to water seepage. These phases will induce de-saturation and re-saturation of all porous media present. Meanwhile, hydrogen gas will be produced within repository tunnels, mainly due to corrosion and water radiolysis. After sealing, gas production within tunnels may lead to pressure increase up to structural breakdown. By allowing propagation of radionuclides, gas leakage would participate to waste dissemination. For such a failure scenario, there is a lack in laboratory data necessary for the varied numerical modelling approaches, which are currently used to simulate the long-term structure performance and sealing ability. In this context, experimentally identifying water retention and gas transport properties through partially-saturated concretes is a crucial issue, together with improving the understanding of the underlying physical phenomena occurring at partial saturation.

In the literature, a number of statistical models is available for concretes, which relate water content w% (or saturation level S_w) to capillary pressure P_{cap}, or to relative humidity (*RH*) through Kelvin's relation (for water retention properties), and, most importantly, water and gas relative permeabilities K_{rw} and K_{rg} to water saturation level S_w (for gas transport properties in the partially-saturated state) [2,3]. The well-known Van Genuchten–Mualem's model [4,5] is certainly one of the most often used for the latter, and it is proposed in a number of articles related to relative permeability of rocks and concretes [6–8]. Such a model may also be used "for lack of anything better", i.e. in the absence of direct measurements of fluid transport properties. These are time consuming and not easy to carry out [9]. On another hand, when actual hydraulic properties are measured, they may be fitted using Van Genuchten's relationship, which is useful for numerical modelling [10]. In this contribution, a key issue is to determine whether a *single* set of Van Genuchten's parameter values is sufficient to fit gas transport data during de-saturation or during re-saturation.

Due to mechanical or thermal loading and to drying shrinkage, concrete may be either sound (intact) or micro-cracked, depending on numerous effects, such as local or global structural restraints [11,12]. In this study, concretes are in their sound state, i.e. they did

* Corresponding author at: ECLille, LML, BP 48, F-59650 Villeneuve d'Ascq, France.
E-mail address: catherine.davy@ec-lille.fr (C.A. Davy).

0008-8846/$ – see front matter © 2012 Elsevier Ltd. All rights reserved.
doi:10.1016/j.cemconres.2012.04.003

not undergo any dedicated treatment intended to micro-crack them. Therefore, these results will be the basis of comparison with identical, yet deliberately micro-cracked, concretes, which involves a whole series of lengthy experiments, see [13]. For special emphasis on water retention properties of *concretes with identical formulation to ours*, which are directly relevant to underground radioactive waste disposal (i.e. at different temperatures of 20, 50 and 80 °C and under partial de-saturation/re-saturation cycling), one may refer to [14–16].

In brief, our contribution addresses the following aspects:

(1) we identify the actual gas relative permeability curves $K_{rg}(S_w)$ for two Andra industrial concretes, named CEMI and CEMV (due to their main cement component); Van Genuchten's model is used to fit these data. All experiments are conducted under moderate hydrostatic pressure, which value (5 MPa) corresponds to the order of magnitude of in situ stresses.
(2) we evaluate the effect of desorption/sorption phases i.e. of how saturation S_w is obtained, on K_{rg}. Indeed, a strong hysteretic effect is generally observed on water retention properties, i.e. on the relationship between water saturation state S_w vs. relative humidity (*RH*), depending on whether it has been obtained during drying or imbibition [17,18]. The legitimate question, which arises from this remark is whether there is also hysteresis in gas relative permeability K_{rg} vs. S_w. Our work answers this question with *direct* experimental results.

One should note here that the main focus of this paper is the effect of water saturation level S_w on gas relative permeability K_{rg}. Variation in S_w is obtained by placing samples at given *RH* until mass stabilisation, which is the easiest method. This also provides sorption/desorption isotherms at ambient temperature. In order to validate our experimental isotherms against existing data, they are compared to other studies on the same concrete formulations, one from our laboratory [16], the other from [14].

2. Experimental methodology

2.1. Concrete materials and samples

Both concretes studied are considered as 'reference concretes' in Andra's programme for disposal design. Two types of cement are used: (1) a CEMI type, which is made of finely ground pure Portland clinker (with setting retardant, i.e. gypsum or anhydrite), and (2) a CEMV/A type, which is constituted of 60 wt.% clinker, 22 wt.% blast-furnace slag, 14 wt.% fly ash and 4 wt.% setting regulator, according to NF EN 196-4 European Standard [19,20]. Blast furnace slag and fly ash are filler and pozzolanic additives to CEMV/A cement. In the following, concrete made with CEMI cement has a water-to-cement ratio (W/C) equal to 0.43, and is called 'CEMI'. Concrete prepared with CEMV/A cement has a (W/C) = 0.39, and it is called 'CEMV'. Table 1 presents both concrete compositions, which correspond to Andra's industrial requirements. Due to both differing cement type and (W/C), CEMI and CEMV mature concretes will have different microstructures, both in terms of pore network and solid skeleton, see [14,16] and Subsection 3.1 here.

Samples are made from a single batch for each concrete type. After 24 h and more, cylindrical samples of diameter Ø = 37.5 mm are cored from larger beams and cut to a length equal to 30 mm. Such size may seem quite small when compared to a maximum aggregate size of 12 mm. Indeed, it would be insufficient to assess concrete mechanical performance. Yet, when measuring hydraulic properties, e.g. gas permeability, it is an adequate compromise: this ensures sample representativeness with regard to the aggregate maximum size, with more than two such aggregates potentially present in the sample height, while limiting the time necessary to reach hydrous equilibrium, see [15,17,21]. In our laboratory, experiments have been performed to evaluate a possible size effect with samples of 65 mm diameter and 30 mm height. These did not show significant differences in gas effective permeability, as compared to those of the present study. To further validate this point, an experimental assessment was performed by J. Verdier et al. [21] on 5–8 concrete samples with a maximum aggregate size of 20 mm. Dry state is obtained at mass stabilisation under 80 °C oven-drying; gas permeability is assessed by imposing a unidirectional gas flow along the cylindrical sample thickness. For samples of 300 mm diameter and 50 mm height, no statistically significant difference in dry gas permeability was found with samples of identical diameter (300 mm) and 100, 200 or 300 mm height. Therefore, study [21] showed that a 50 mm height sample is sufficient to measure gas permeability of concretes with a maximum aggregate size of 20 mm. In the present study, we use a 12 mm maximum aggregate size and 30 mm sample height for permeability measurements, which is comparable to [21]: we have an identical (maximum aggregate size/sample height) ratio of 0.4.

After coring and cutting, samples are cured in lime-saturated water at 20 °C for six months before use. Therefore, we consider that the hydration process is sufficiently complete so that concrete microstructure will not vary significantly during testing [12,15,17,21]. Moreover, concretes are assumed to be fully water-saturated at the end of this cure.

2.2. Experimental strategy

To conduct the experimental programme, we have selected eight water saturation levels S_w, obtained at mass stabilization, by placing samples in hermetic chambers over salt-saturated solutions, which impose respective *RH*s of 98, 92, 85, 75, 70, 59, 43 and 11%.

2.2.1. Choice of a reference dry state

The dry state, considered to be the reference state at which intrinsic gas permeability is measured, is obtained after oven-drying at 60 °C until mass stabilization. Two different climatic chambers run at 60 °C have been tested for relative humidity for 24 h: *RH* values range between 6.6 and 7.2%, for actual temperatures ranging from 55 to 65 °C.

There is a long-lasting debate concerning the adequate method to be used to obtain the dry state, which also provides conventional porosity [22]. Vacuum-drying, oven-drying at 60/65 °C or 100/105 °C and freeze-drying are the most popular methods. If, as is regularly recommended, 105 °C is used as the drying temperature, thermally-induced cracks may occur, as well as a first degradation of hydrates, such as ettringite, which decomposition is attested above 70 °C

Table 1
Concrete compositions.

	CEMI			CEMV		
Component	Nature	Source	Amount [kg/m^3]	Nature	Source	Amount [kg/m^3]
Cement	CEMI 52.5 R	Lafarge, France	400	CEMV/A 42.5 N	Calcia, France	450
Sand	Limestone [0–4 mm]	Boulonnais quarry, France	858	Limestone [0–4 mm]	Boulonnais quarry, France	800
Gravel	Limestone [5–12 mm]	Boulonnais quarry, France	945	Limestone [5–12 mm]	Boulonnais quarry, France	984
Super-plasticizer	Glenium 27	BASF	10	Glenium 27	BASF	11.5
Water	–	–	171	–	–	176.3
W/C	0.43			0.39		

[22,23]. On another hand, very moderate drying, below 60 °C, may not lead to complete material de-saturation, i.e. it will not provide actual porosity and gas intrinsic permeability values. Vacuum drying leads to similar micro-structural modifications as 60 °C oven-drying, and freeze-drying leads to significant, although limited, micro-structural damage [22].

The dry state obtained after mass stabilization at 11%*RH* was not selected as the reference state: it corresponds to a similar procedure as vacuum-drying, and hence, it is bound to imply similar micro-structural modifications, and it is longer to obtain than 60/65 °C oven-drying. A compromise had to be made, especially to perform intrinsic permeability measurements (followed by sample re-saturation) in a limited time frame, and it was in favour of the moderate 60 °C oven-drying. In fact, a little adsorbed water may remain when concrete is dried at 60 °C. Yet, this water, if present, is not reputed to have a significant effect on gas flow i.e. on gas permeability [24].

2.2.2. Choice of a de-saturation/saturation process — test representativeness

Two main possibilities were considered to obtain partial water saturation, prior to gas transport assessment. The first one was to follow the same sample along its whole de-saturation process, from the initial fully water-saturated state to the reference dry state, such as in [16]. Study [16] was solely on desorption isotherms: it has started five years ago, and samples are not yet mass stabilized at 30%*RH* and 20 °C. In such case, gas effective permeability would have been measured after each *RH*-drying step, each one lasting several months. Therefore, it is highly time consuming [12,16] and, if the sample under test is atypical, e.g. if it comprises a great number of air voids, the whole set of results cannot be exploited. Moreover, due to extensive test duration, a greater risk exists to get parasitical phenomena, like enhanced structural micro-cracking, carbonation etc. [25]. As a consequence, we have chosen to test one different sample at each *RH* level, once during de-saturation, once in the dry state, and three times during re-saturation, at different time intervals. With this choice, the whole experimental programme has lasted ca. two years and a half (900 days).

Transport experiments amount to five values of apparent gas permeability per sample (except for those in the reference dry state). All are performed under identical hydrostatic stress, see the triaxial cell and its associated gas panel in Fig. 1. This leads to better statistical values of relative gas permeability K_{rg}, because it provides four K_{rg} values per sample, at different water saturation levels. As nine samples were used for each concrete (CEMI and CEMV), comprising one in the reference dry state, we have measured 40 effective gas permeability values per material (plus one value in the dry state). Of these 40 values, 8 are obtained during de-sorption, 8 in the dry state and 24 during sorption; this leads to 64 relative gas permeability values for the two concretes. In brief, this experimental campaign has required a total number of 82 permeability experiments in the triaxial confining cell. This is considered sufficient to provide proper material representativeness and reliability of our results. In parallel, the experiments provide 9 porosity values per material, which is also assumed sufficient to get proper material representativeness. Complementarily, dry gas permeability and porosity measurements are compared to those of other studies [14,16].

2.2.3. Complete experimental procedure

Except for oven drying, all experiments are performed at a mean temperature of 22 °C in an air-conditioned room, as in [15,17,26]. The whole experimental procedure is as follows:

1. All samples are cured in lime-saturated water for 6 months. The initial state after curing is assumed to be the fully water-saturated state. Each sample mass is then M_w.
2. Each sample is placed in a different hermetic chamber under the prescribed *RH*% (or in the oven at 60 °C). Its weight is monitored regularly.
3. Mass is assumed to be stable when its variation is less than 0.01 g during three successive days, for an initial mass of around 80 g. Stabilised mass is noted M_s. At mass stabilisation, effective permeability gas $K_{eff}(RH)$ is measured using a high gas pressure value (see paragraph 4 for details). For all samples except the dry ones, saturation level S_w is not known yet (dry mass has not been assessed at this stage). For dry samples, effective gas permeability is intrinsic gas permeability, and S_w is 0.
4. After gas permeability measurement at given *RH*, the sample is dried at 60 °C until mass stabilisation, using the same criterion as in 3. (See above.). M_d is sample dry mass, obtained after this step. For each sample, this provides its total connected, or conventional, porosity, which is defined as the ratio between the total pore volume and the sample volume, i.e.:

$$\phi = \frac{V_p}{V_{sample}} = \frac{M_w - M_d}{\rho_w V_{sample}} (\%) \quad (1)$$

where V_{sample} is sample volume and ρ_w is water specific mass.

Water saturation level S_w is defined as the ratio between the

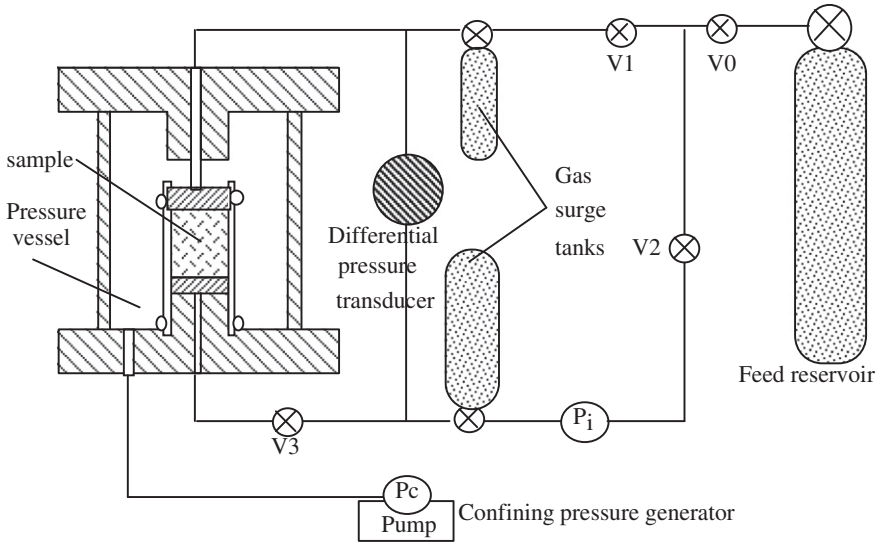

Fig. 1. Diagram of the experimental set-up (triaxial cell and gas panel).

volume of pores filled with water, and the total pore volume, so that it is obtained at given *RH* as:

$$S_w(RH) = \frac{V_p^{water}}{V_p} = \frac{M_w - M_s(RH)}{M_w - M_d} \quad (2)$$

S_w represents the proportion of pore volume filled with water. Alternatively, when full saturation state is unknown, mass water content $w(\%)$ may be used, which is defined as:

$$w = \frac{M_s(RH) - M_d}{M_d} \quad (3)$$

Intrinsic gas permeability K_{int} is the effective gas permeability in the dry state, taken at a high gas pressure value (see below for details). For each sample at given S_w, relative gas permeability K_{rg} is deduced from:

$$K_{rg}(S_w) = \frac{K_{eff}(S_w)}{K_{int}} \quad (4)$$

Due to its definition, K_{rg} varies in the range [0;1] whatever the sample considered; 0 is for the fully water-saturated case and 1 for the dry one. It is generally admitted that relative gas permeability K_{rg} does not depend on the nature of the (partially) saturating liquid [27] and that it is mainly a function of saturation state S_w [28]. It may also depend on the gas nature [29]. Argon was chosen here, as it is a common inert gas, and for several other reasons, see Sub-section 2.3.

After intrinsic gas permeability measurement, the sample is subjected once again to its previous *RH*% level, in order to evaluate the hysteretic effect of the cycle drying → re-saturation and to measure its effective gas permeability at this new re-saturation state. During re-saturation, three distinct measurements were performed at different times of 80, 380 and 540 days, therefore spanning between one and two years time.

2.3. Measuring gas permeability

Preliminarily to this study, gas permeability tests have been performed on a CEMV sample successively dried at 60 °C and 105 °C. Helium has been used as the interstitial fluid after 60 °C and 105 °C drying, and compared with argon after 105 °C drying. First, Fig. 2 shows that there is no significant difference in helium gas permeability when the sample is successively dried at 60 °C and 105 °C. Further, both gases have been flown through the sample at different pressures to account for Klinkenberg's slippage effect, i.e. for the fact that gas molecules slip on the pore wall surfaces, providing varying permeability with varying gas pressure [30–32]. When assuming a uni-dimensional and quasi-static gas flow through a dry sample, Klinkenberg's equation is written as follows:

$$K_{app} = K_{eff} = K_{int}(1 + b/P_m) \quad (5)$$

where K_{app} is apparent (or effective) gas permeability measured at the average gas pressure P_m through the sample; β is Klinkenberg's coefficient, and K_{int} is dry, or intrinsic, gas permeability. K_{int} is determined as the Y-intercept in a diagram plotting apparent gas permeability $K_{app} = K_{eff}$ vs. $(1/P_m)$, see Fig. 2. K_{int} is of 0.72×10^{-17} m^2 for argon and 0.81×10^{-17} m^2 for helium. This represents a difference of 0.09×10^{-17} m^2, i.e. 12.5% for K_{int} assessed with argon, and 11.1% for K_{int} assessed with helium. This difference in K_{int} is considered sufficiently limited to justify to keep argon all through the following study. Further, a lower slope for $K_{app}(1/P_m)$ is recorded with argon than with helium: apparent gas permeability K_{app} varies half as much with inverse

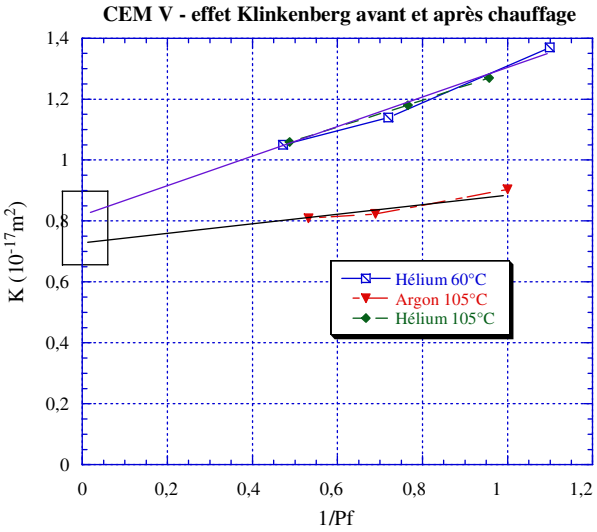

Fig. 2. Influence of static gas pressure on effective gas permeability, when using either helium or argon, for a CEMV concrete sample successively dried at 60 °C and 105 °C. Plot shows the evolution of effective (or apparent) gas permeability $K = K_{eff}$ (expressed in 10^{-17} m^2) vs. the inverse of average gas pressure $(1/P_f) = (1/P_m)$ (expressed in MPa^{-1}).

average pressure $(1/P_m)$ if argon is the injected gas, i.e. a more limited Klinkenberg's effect is identified in this pressure range if argon is preferred to helium. As expected, Klinkenberg's gas slippage effect occurs more significantly with smaller helium molecules than with argon, while the resulting intrinsic permeability, obtained when $(1/P_m)$ tends towards 0, presents limited difference between both gases.

All through this work, we apply the pulse-test method, which has been used in our laboratory for a number of years. Its principle is to subject the cylindrical sample to a moderate confining pressure $P_c = 5$ MPa, simultaneously to a stable static gas pressure P_s on both its upper and lower sides. Then, at time $t = 0$, a slight gas pressure excess $\Delta P(t = 0)$ is applied on one of the sample sides. The evolution of the difference in gas pressure between both sample sides $(P_1 - P_2)$ is recorded over a period of time, and provides effective gas permeability, see Fig. 1. This test may be labelled as a low amplitude pulse test [33], designed to avoid significant sample de-saturation during gas flow. This has been validated experimentally by weighing each sample, before and after permeability test: no significant mass variation was recorded.

The experimental device comprises:

- A confining cell;
- A Gilson pump and a digital manometer capable of recording the applied confining pressure;
- A gas injection panel comprising:
  - An argon gas feed reservoir and a high-pressure reducer manometer;
  - Two surge reservoirs R1 and R2: the sample is placed between them;
  - A digital manometer for measuring static pressure P_s;
  - A transmitter and a differential pressure indicator to measure the difference in pressure $(P_1 - P_2)$ between both sample sides;
  - A computer (not shown in Fig. 1) for recording the difference in pressure $(P_1 - P_2)$ over a period of time.

As detailed in [27], the difference in pressure between both sample sides is fitted satisfactorily by:

$$P_1(t) - P_2(t) = \Delta P(t) = \Delta P_1 \exp(-cP_f t) \quad (6)$$

$$\text{with } c = -\frac{K_{eff}(S_w)A}{\mu h}\left(\frac{1}{V_1}+\frac{1}{V_2}\right). \quad (7)$$

V_1 and V_2 are the volumes of the surge reservoirs located on each sample side, A is sample cross section, h is sample height, μ is gas viscosity (2.2×10^{-5} Pa/s for argon) and P_f is the final pressure which, as $V_1 = V_2 = 0.4$ l in the present case, is close to $(P_1(t=0)+P_2(t=0))/2$. On each sample side, at time $t=0$, gas pressures are respectively $P_1(t=0) = P_s + \Delta P(t=0)$ and $P_2(t=0) = P_s$, where P_s is the initial static pressure. In fact, Eq. (6) is applicable if volumes V_1 and V_2 are much larger than the sample pore volume [34], which is obviously the case here with the choice of 0.4 liter reservoirs. The choice of gas pressure values P_s and $\Delta P(t=0)$ have been guided by two constraints:

- No significant sample de-saturation is to occur during gas permeability tests
- Klinkenberg's effect has to be sufficiently limited to avoid multiple measurements

To mask Klinkenberg's effect, a high static pressure has to be applied [35]. To assess its value, our preliminary test is used. Fig. 2 plots effective gas permeability vs. the inverse of $P_m = P_f = (P_1(t=0) + P_2(t=0))/2$. It is observed that with argon gas, a static pressure value $P_s = 2$ MPa (which corresponds to $(1/P_f) = 0.5$) provides K_{app} $(1/P_m = 0.5) = 0.8\times10^{-17}$ m^2 while $K_{int} = 0.72\times10^{-17}$ m^2: K_{app} is close to K_{int}. Their difference represents 11% of K_{int}. Therefore, in the following, for *every* permeability test on CEMI and CEMV concretes, $P_s \approx 2$–2.2 MPa (i.e. $(1/P_f) = 0.45$–0.5). This also ensures that all permeability measurements may be compared on the same basis.

Moreover, the initial difference in pressure (i.e. the pulse test amplitude) is fixed at $\Delta P(t=0) = 0.3$ MPa, which is one order of magnitude lower than static pressure P_s.

3. Results

3.1. Gas transport properties in the dry state: porosity and intrinsic gas permeability

3.1.1. Porosity

Fig. 3 displays porosity values for 9 samples of each concrete. X-axis label corresponds to the *RH* to which each sample has been subjected to. The main observation is the homogeneity in porosity for both materials, as also attested by the low standard deviations: average porosity ϕ is 8.3% for CEMI concrete, with a standard deviation representing 5.8% of the average, and ϕ = 10.3% for CEMV concrete, with a standard deviation representing 7.2% of the average.

As a matter of comparison, for different batches of the same concrete formulations as in this study, Brue et al. [16] obtain very similar values to ours for CEMI concrete, with an average connected porosity ϕ = 8.1% for 60 °C oven-dried material, and a standard deviation representing 11% of the average; for 60 °C oven-dried CEMV concrete, ϕ is significantly greater than in this study, with an average value of 11.9%, and a standard deviation limited to 5.9% of the average. As for Ranaivomanana et al. [14], after one year water curing and 105 °C oven-drying, CEMI concrete porosity is of 12.3% (for which Brue et al. [16] have a lower value of 10.1%); CEMV concrete porosity is of 14.7%, for which Brue et al. [16] have assessed a slightly greater value of 15.3% +/− 0.4. For CEMI only, Poyet [15] measures greater connected porosity than Brue et al. [16] after drying at 60 and 105 °C, with values at 11.3% and 12.3% respectively. To conclude, a significant effect of the concrete batch, and of the drying temperature, is observed for porosity measurements of both materials.

3.1.2. Dry intrinsic gas permeability

Let us now analyse dry (intrinsic) gas permeabilities. In this study, for CEMI concrete, intrinsic gas permeability ranges between 2×10^{-18} m^2 and 4.4×10^{-18} m^2 at 5 MPa confinement. On one single CEMI concrete sample, Brue et al. [16] obtain a slightly greater value of 5×10^{-18} m^2 at 5 MPa confinement. For CEMI concrete, Poyet [15] measures an intrinsic gas permeability of 2×10^{-17} m^2 (average on three samples). This value, obtained without sample confinement (which would close up micro-cracks), is an order of magnitude greater than our values. This was expected for the concrete batch in [15], which has significantly greater porosity (11.3%) than ours (8.3%).

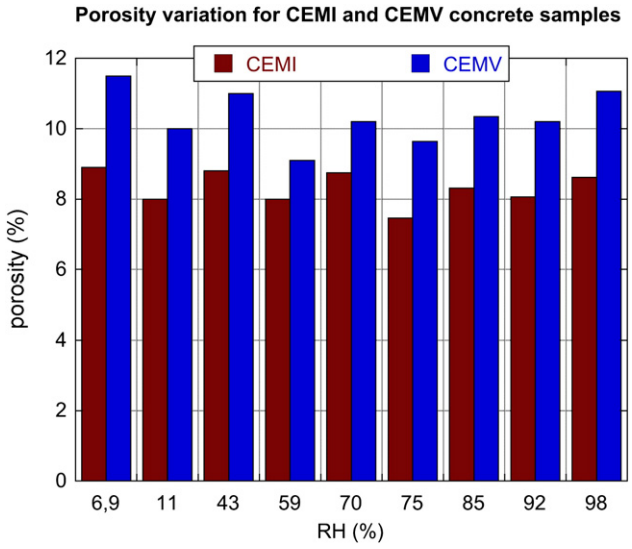

Fig. 3. Porosity distribution for the whole sample set (CEMI and CEMV). Sample number corresponds to the *RH* it has been subjected to.

In Fig. 4, intrinsic gas permeability K_{int} is plotted v.s. porosity ϕ. A clear correlation between K_{int} and ϕ is observed for pure Portland cement-CEMI concrete: its permeability is consistently lower for less porous samples (Pearson's coefficient R2 is of 79.8%). Similarly, Van den Heede et al. [36] identify a linear relationship between dry gas permeability and porosity, yet for high-volume fly ash concrete. Also, in [36], while porosity is high (with values ranging from 14 to 17%), gas permeability values are on the order of 10^{-16} m^2, which is two orders of magnitude greater than for our concretes, making actual comparison delicate.On the contrary, no correlation between K_{int} and ϕ is observed for CEMV concrete, see Fig. 4 (Pearson's coefficient R2 is of 16.7%). The latter is evidence that there is no systematic link between porosity and permeability, as previously shown, e.g. in [37]. On another hand, even if CEMV concrete is more porous than CEMI,

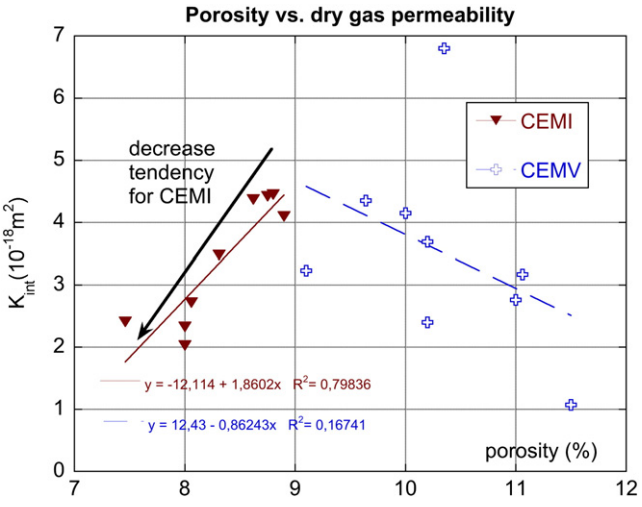

Fig. 4. Porosity v.s. intrinsic dry gas permeability.

both have similarly low dry gas permeabilities: the mean value for K_{int} is 3.4×10^{-18} m^2 ($+/-0.9\times10^{-18}$ m^2) for CEMI concrete and 3.5×10^{-18} m^2 ($+/-1.1\times10^{-18}$ m^2) for CEMV concrete.

3.2. Water retention properties

3.2.1. Mass variation kinetics

For both concretes, Figs. 5 and 6 present relative mass variations vs. time, for the first 200 days (Fig. 5) and for the whole experiment duration of 900 days (Fig. 6), for (a): CEMI concrete and (b): CEMV concrete. The three phases of our experiment are presented: for each sample, placement at given *RH*, 60 °C oven-drying and re-saturation at an identical *RH* as in the first phase.

In a consistent manner whatever the *RH*, drying and re-saturation kinetics are significantly greater for CEMI than for CEMV. For instance, for a sample under 60 °C oven-drying at the test start, CEMI concrete requires 23 days to reach stable mass, whereas 100 days are necessary for CEMV; for a sample mass-stabilised at 98%*RH*, it takes 38 days for CEMI to reach the reference dry state, and 120 days for CEMV. Under 98%*RH*, CEMI takes 477 days to re-saturate from the dry state, whereas CEMV requires 538 days. As expected, for initially water saturated samples, the greater the *RH*, the quicker the mass stabilization, for both concretes; for reference dry samples, the greater the *RH*, the slower the re-saturation kinetics.

Mass loss variations display several particular features. First, initially water-saturated CEMV concrete loses less mass than CEMI when subjected to $RH \in [11;98]$ %. This is attributed to a greater number of small pores in CEMV than in CEMI, which retain more water down to low *RH*, see Sub-section 3.2.3 for detailed analysis on this aspect. For instance, for samples subjected to 11% *RH*, mass loss is of 2.33% for CEMI and 2% for CEMV; at 70% *RH*, it is of 1.5% for CEMI and 0.8% for CEMV; at 98%*RH* it is only of 1% for CEMI and 0.34% for CEMV. Therefore, CEMV water retention capacity is greater than that of CEMI. Despite this, after full drying in the oven at 60 °C, CEMV loses more mass than CEMI: CEMV total water content is greater than that of CEMI. This was expected, due to the greater total porosity of CEMV compared to that of CEMI see Fig. 3. At the dry state, for each concrete taken individually, total mass loss varies

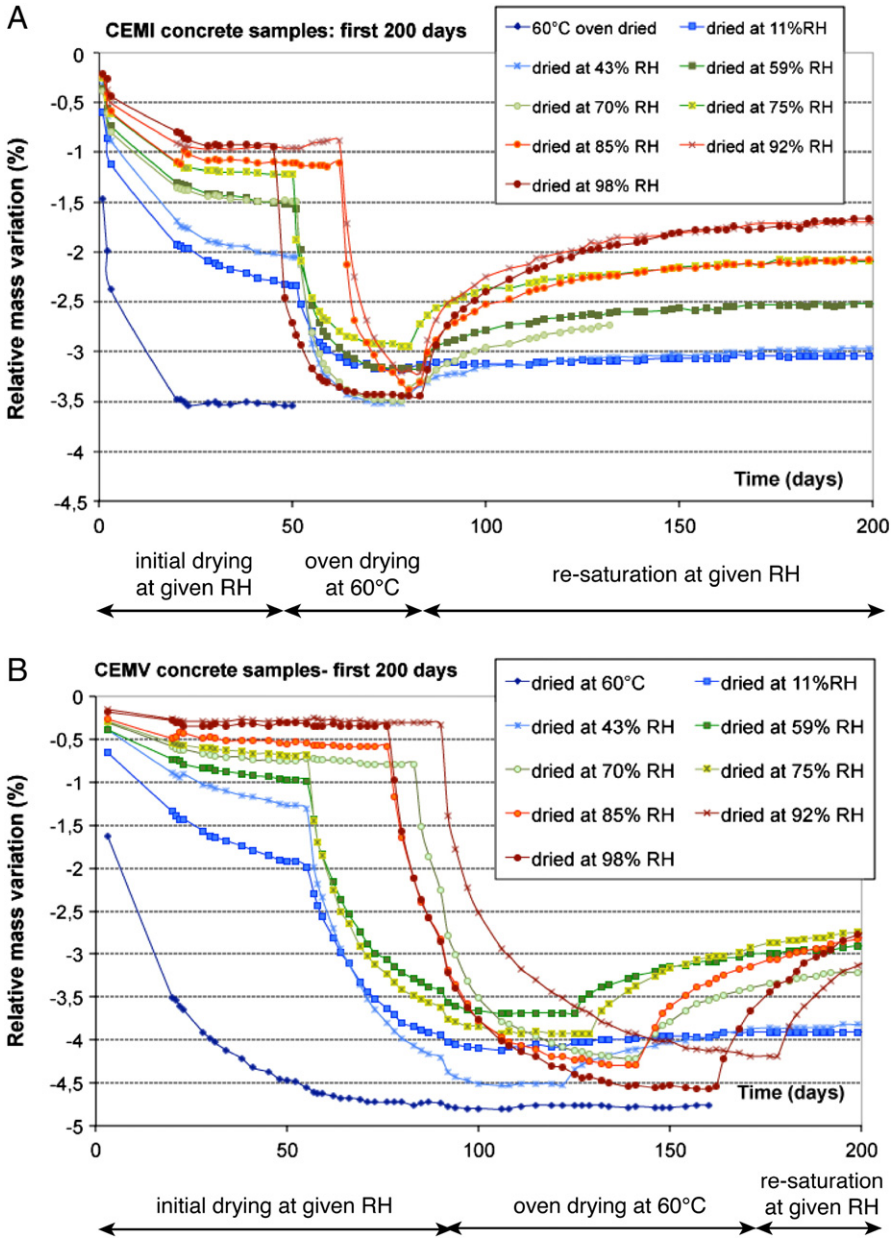

Fig. 5. Drying kinetics for the first 200 days for (a) CEMI samples; (b) CEMV samples.

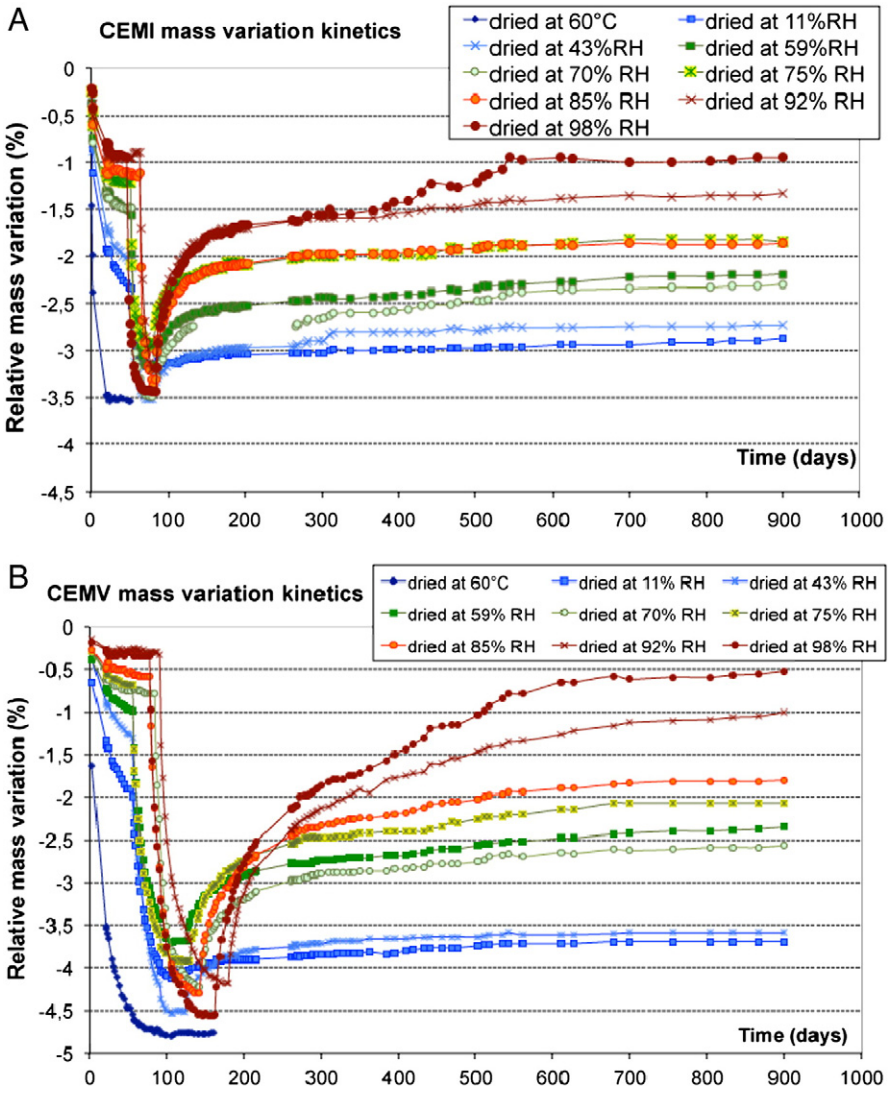

Fig. 6. Drying and re-saturation kinetics for the whole 900 day experiment for (A) CEMI concrete samples; (B) CEMV concrete samples.

significantly between the different tested samples: it ranges between 3% and 3.5% for CEMI and 3.7% and 4.8% for CEMV. Nevertheless, this means that total mass loss variation is greater for CEMV than for CEMI. Upon re-saturation, and contrarily to CEMI, CEMV does not reach back mass variation levels obtained after the first de-saturation step (from initially water-saturated down to mass stabilised at given *RH*). This means that either water takes longer time to re-integrate the pore network than these experiments have allowed, or that all water could not retrieve its former position after full drying, as proposed by Jennings [38], see Sub-section 3.3.2 for detailed analysis on this point.

3.2.2. De-sorption phase

First de-sorption isotherms are plotted in Fig. 7 for both concretes. They are compared to first de-sorption curves by Ranaivomanana et al. [14] and Brue et al. [16] in Fig. 8, which is directly derived from [16]. Except for higher *RH* (>95%) at which the effect of air voids or large capillary pores is predominant, all first desorption isotherms follow similar evolutions, although they were obtained with different concrete batches and/or in different laboratories.

Despite using the same experimental procedure all along this study, a strong difference is observed between both concretes, see Fig. 7. Firstly, for CEMV, one notes a very high irreducible saturation level down to very low relative humidities, with $S_w = 72\%$ at $RH = 43\%$ and $S_w = 53\%$ at $RH = 11\%$. For CEMI, $S_w = 41.6\%$ at $RH = 43\%$, and 26.6% at $RH = 11\%$. This may be translated in terms of smallest drained pore diameter, by a simplified analysis, as follows.

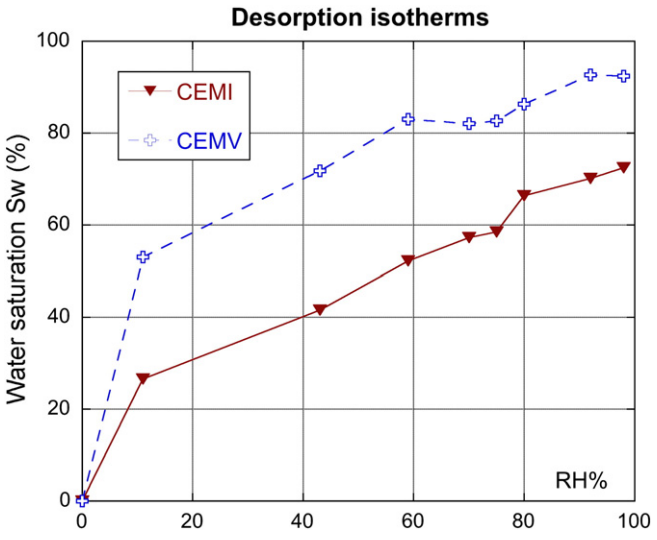

Fig. 7. Comparison of first de-sorption curves for CEMI and CEMV concretes at 20 °C.

Kelvin–Laplace's equation applied to water allows the calculation of the smallest drained pore diameter d^i at given temperature T and for given humidity conditions, as:

$$d^i = -\frac{4\gamma_w(T)M_w}{\Re T\rho_w(T)\ln(RH)} \quad (8)$$

where ρ_w is water specific mass (function of temperature T) [kg/m^3]; $\Re$ is the perfect gas constant [J/mol.K]; T is temperature [K] ; M_w is water molar mass [kg/mol] and γ_w is the surface tension of water/air (also a function of temperature) [39]. The sole Kelvin's relation provides capillary pressure P_{cap} as:

$$P_{cap} = -\frac{\rho_w}{M_w}\Re T\ln(RH). \quad (9)$$

If we assume that Kelvin–Laplace's capillary law applies for the smallest concrete pores, our results mean that, at 43%*RH*, 72% of the water present in CEMV concrete (and only 41.6% for CEMI) lies in pores with a radius smaller than 2.5 nm, i.e. within C–S–H nano-porosity [40]. This calculation is mainly qualitative, as it is well known that water confined in nano-pores is adsorbed water, strongly bound to the pore walls [24,41], which is not accurately described by capillary Kelvin–Laplace's law (capillary pores within a concrete material are above 50 nm [24,42]). However, this implies that the pore microstructure of CEMV concrete comprises a non negligible amount of much thinner pores than those of CEMI, with 30.4% more water present at 43%*RH* than in CEMI. Indeed, CEMV cement contains pozzolanic species, which, on the long term, results in a greater amount of C–S–H (mainly created from pozzolanic reactions with portlandite), and thus, to a greater amount of fine C–S–H porosity [43], see also Sub-section 3.3.2 on this point.

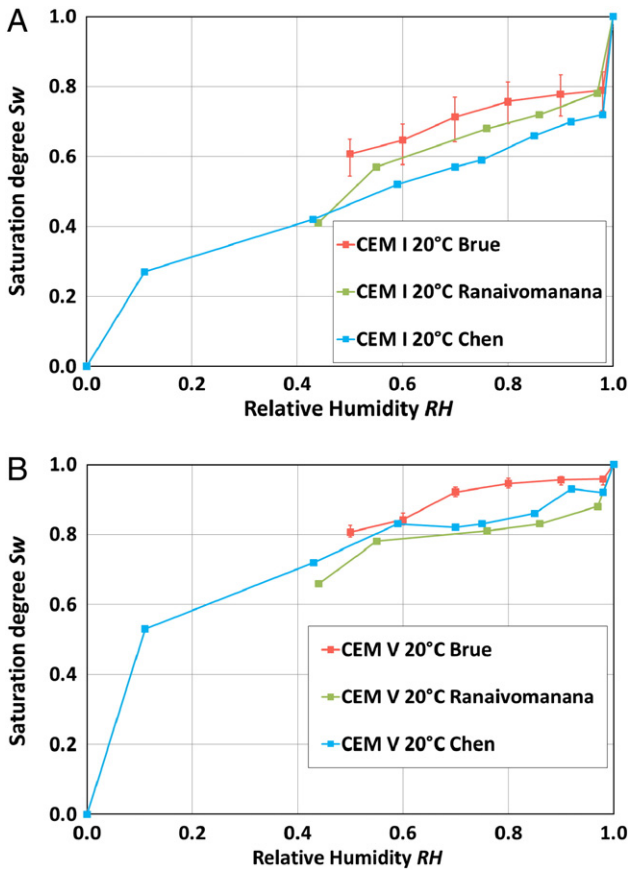

Fig. 8. Comparison of first desorption isotherms for three different batches of (A): CEMI concrete, (B): CEMV concrete, from this study (labelled 'Chen'), [11] (labelled 'Ranaivomanana') and [13] (labelled 'Brue'), all at 20 °C. Both figures are from [13].

3.2.3. Desorption isotherms and concrete microstructure

Although from a different batch than here, the pore microstructure of CEMI and CEMV concretes has been identified by MIP in [16]. Three main peaks in pore size distributions are observed: the greater is centred around 1–2 μm, and corresponds to large capillary pores, entrapped air bubbles and/or to micro-cracks; the second peak is centred around 200 nm for CEMI and 400 nm for CEMV, and is attributed to capillary pores [24,42]; the third, greatest peak is centred around 30 nm for CEMI and 40 nm for CEMV. The latter is attributed to pores located in non-crystalline areas, between C–S–H layers (inter-layer pores) [40]. Being non accessible to usual MIP (>6 nm pore size range), intra-layer C–S–H pores (2–5 nm size range) are not observed. Nevertheless, for CEMV concrete, the pore volume corresponding to the area under the third peak (20–40 nm) is greater than for CEMI: this means that a greater number of small inter-layer C–S–H pores is present in CEMV than in CEMI. This has been consistently observed on three different samples of each concrete, see [44]. This greater amount of C–S–H pores is attributed to pozzolanic additions in CEMV/A-type cement, which react with portlandite to form further C–S–H than in CEMI.

Complementarily, it is interesting to compare sorption curves – obtained from an initially dry state – for both concretes, at the beginning of the process, as the increase in mass in the lower *RH* range is generally attributed to adsorbed water [41,45]. Using the BET theory for the first adsorbed water layer, one evaluates the specific surface of the porous structure from the following relation [15,45,46]:

$$\frac{RH}{(1-RH)w} = \frac{1+(C-1)RH}{Cw_m} \quad (10)$$

where C is a constant, which depends on the material considered, and w is the current water content (expressed in %). w_m is the water content when the first adsorbed layer covers the whole specific surface of pores. If $\frac{RH}{(1-RH)w}$ is plotted v.s. *RH*, a linear relationship is obtained if the BET theory applies, with a slope of $\frac{C-1}{Cw_m}$ and a Y-intercept of $\frac{1}{Cw_m}$ [45]. In practice, as long as $\frac{RH}{(1-RH)w}$ vs. *RH* is a linear relation, it is admitted that the BET theory applies. Hereafter, we analyse $\frac{RH}{(1-RH)w}$ vs. *RH* in its linear part only, in order to evaluate the specific surface of the pore microstructure. Fig. 9 represents $\frac{RH}{(1-RH)w}$ vs. *RH* for both concretes. As expected, one observes that the BET theory applies in the *RH* range [0;0.43] whatever the material considered. These results are in good agreement with those found by e.g. Baroghel Bouny [17]. As a consequence, the specific pore surface is calculated with the experimental points obtained at 11 and 43% *RH* only. The effective monomolecular thickness of water is generally assumed equal to $e_m = 3.1$ Å [45,47]. If A is the specific pore surface, we obtain $w_m = \rho_w A e_m$ [45], from which we calculate:

- For CEMI: A = 18 m^2/g
- For CEMV: A = 20 m^2/g

As a matter of comparison, MIP measurements provide smaller values of only 2.35 m^2/g for CEMI concrete and 4.88 m^2/g for CEMV concrete [16]. This is not surprising because mercury cannot explore the thinnest porosity [48]. Nevertheless, both methods show that the specific pore surface of CEMV is higher than that of CEMI, in good agreement with desorption results, see Fig. 7: CEMV has a greater water retention ability than CEMI. This is attributed to a greater C–S–H amount in the microstructure of CEMV than in that of CEMI, which leads to a greater amount of fine porosity (2–5 nm for intra-layer C–S–H pores and 14–30 nm for inter-layer pores [40]), with a higher specific surface.

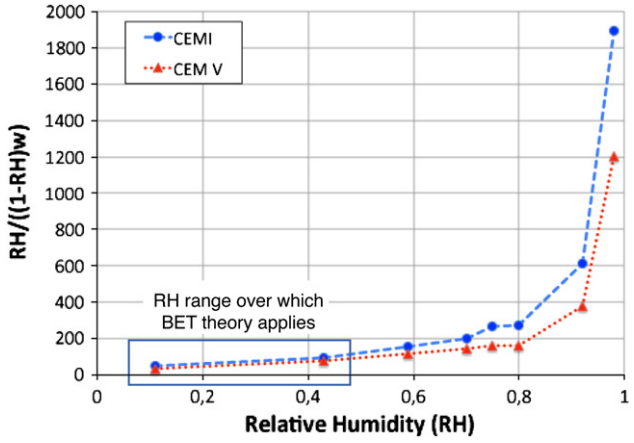

Fig. 9. Plot of $\frac{RH}{(1-RH)w}$ vs. *RH*, presented in order to assess the *RH* range over which the BET theory applies for CEMI and CEMV concretes. This curve displays the expected linear relationship up to 43%*RH*.

Finally, by considering a simplified stoichiometric model for the cement paste, which accounts for partial hydration and for each cement composition, Ranaivomanana et al. [14] provide 0.098 m^3 C–S–H/m^3 for CEMI concrete, and 0.115 m^3 C–S–H/m^3 for CEMV concrete. Different computations, and sorption experiments on CEMI and CEMV cement pastes by Drouet [49] also support the presence of a greater C–S–H amount in CEMV than in CEMI. As C–S–H have finer pores than other constituents of the microstructure, CEMV concrete has a greater amount of fine (2–50 nm) pores than CEMI, together with a higher total porosity [14,43,50,51].

3.2.4. Re-saturation phase

Re-saturation results for CEMI are given in Fig. 10, and those for CEMV are in Fig. 11, together with de-sorption curves. A strong hysteretic behaviour is observed for both materials, except at the highest relative humidity levels. At *RH* = 98%, CEMI recovers the saturation level reached during initial de-sorption, whereas CEMV stabilizes at a saturation slightly below that obtained during de-sorption. The latter may completely disappear given further time (more than the current 490 days). In the intermediate *RH* range, i.e. between 11 and 92%*RH*, a significant difference in saturation S_w is obtained between de-sorption and sorption phases: for CEMI concrete, a difference of up to 24% in S_w

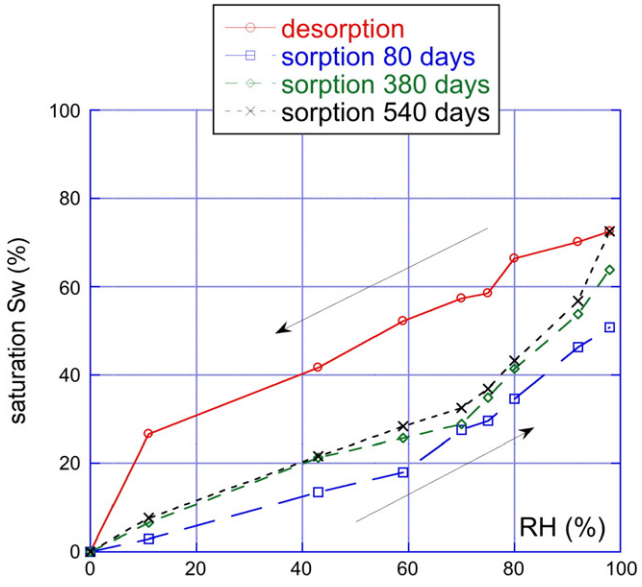

Fig. 10. Desorption and sorption curves at different imbibition durations for CEMI concrete.

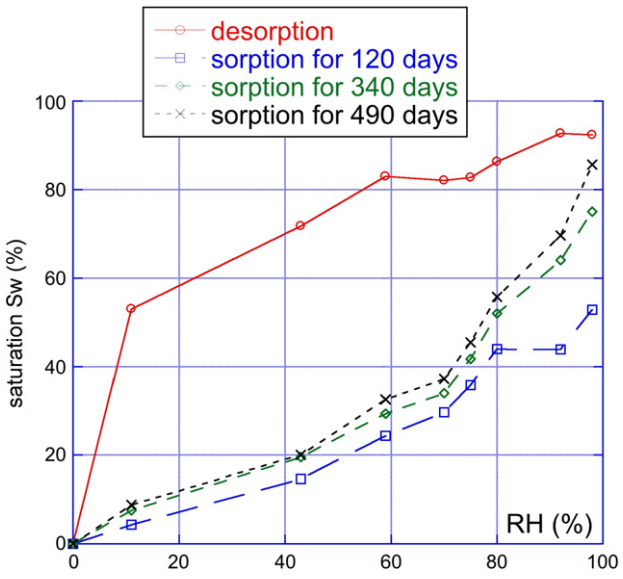

Fig. 11. Desorption and sorption curves at different imbibition durations for CEMV concrete.

is observed between de-sorption and re-saturation at given *RH*; for CEMV concrete, the maximum difference in S_w at given *RH* is of 52%. This well-known hysteresis may be attributed to bottle neck effects within the pore network, whereby small pore throats block water access to bigger pore sizes, so that water re-saturation becomes more difficult after full drying (i.e. during re-saturation phase), see [48,52]. Other interpretations are proposed in Sub-section 3.3.2. These comprise the existence of micro-cracks, carbonation, the influence of capillary pressure, or phenomena occurring at the C–S–H scale.

3.3. Effective and relative gas permeability

Our results have shown that CEMV concrete is more porous than CEMI, while their intrinsic (dry) gas permeability is similar. De-sorption–sorption processes have provided isotherm curves marked by significant hysteresis. For CEMV concrete, higher water retention at low *RH* is evidence of a greater number of thin pores (2–50 nm) than CEMI; this is also correlated by MIP measurements [16]. Due to these, strong differences between CEMI and CEMV are expected in their effective (or relative) gas permeability at varying water saturation level.

3.3.1. De-sorption phase

First results, obtained during desorption *only*, are given in Fig. 12: effective gas permeability is compared with varying S_w for both concretes. Results are consistent, as a clear increase in gas permeability is

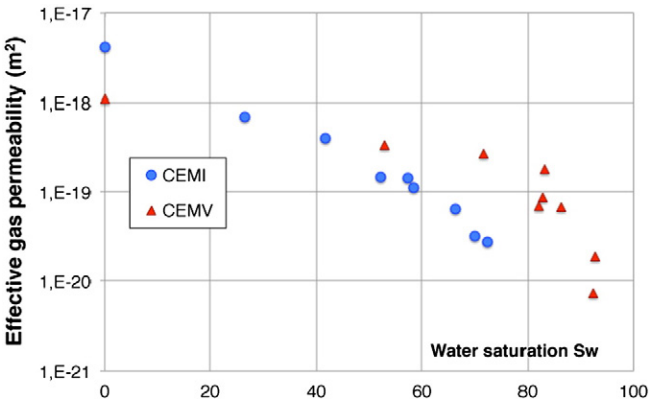

Fig. 12. Effective gas permeability $K_{eff}(S_w)$ for both concretes — de-sorption phase only.

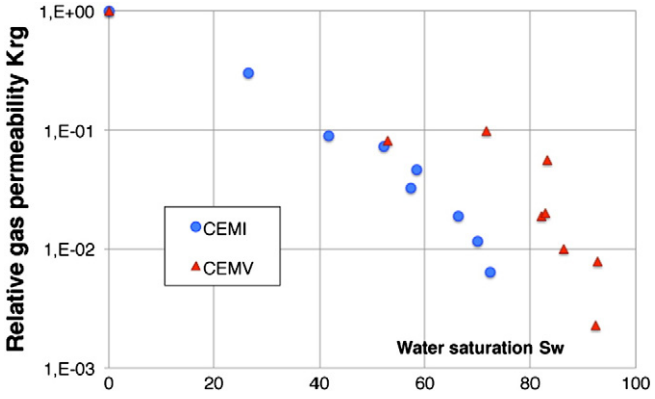

Fig. 13. Relative gas permeability $K_{rg}(S_w)$ for both concretes — de-sorption phase only.

measured as water saturation S_w decreases [28]. K_{eff} values range between $[2.7\times10^{-20}; 4.1\times10^{-18}]m^2$ for CEMI concrete and in a lower $[7.2\times10^{-21}; 1.7\times10^{-18}]m^2$ range for CEMV concrete. Comparison is easier, in a similar [0;1] range, in a relative gas permeability K_{rg} diagram. K_{rg} results are given in Fig. 13 for both concretes, also during the *sole* de-sorption phase.

First, it is observed that experimental points for CEMI and CEMV concretes cannot be fitted by the same curve: CEMV concrete displays a sharp increase in permeability at the start of de-saturation, with two orders of magnitude increase in the range [80%;100%], see Figs. 12 and 13. For CEMI concrete, the increase in permeability is almost linear, and more progressive than for CEMV. At given permeability, the saturation level is consistently lower for CEMI than for CEMV, down to $S_w<50\%$. For instance, a low gas permeability $K_{eff}=10^{-19}\,m^2$ corresponds to $S_w=59\%$ for CEMI concrete, whereas $S_w=81$–84% for CEMV. Alternately, $K_{rg}=0.02$ is associated to $S_w=66\%$ for CEMI concrete, and $S_w=82.1$–82.7% for CEMV. This means that CEMV concrete retains greater water amounts despite similar gas transport ability as CEMI concrete. This greater water amount in CEMV does not actually participate in gas flow, possibly because it is located within thin C–S–H pores.

Further, relative gas permeability K_{rg} lies in the higher range of [0.1;1] for S_w decreasing from 42% to 0% for CEMI, and from 72% to 0% for CEMV. The limits at $S_w=42\%$ (CEMI) and 72% (CEMV) are both obtained for $RH=43\%$. As in Sub-section 3.2.2 (on desorption and water retention), if Kelvin–Laplace's relation applies, this result means that 90% of the gas flow (obtained in the range [0.1;1]) occurs in pores of diameter d^i less than 2.5 nm (drained from 43%*RH* and below). These are not capillary, but C–S–H pores, see Sub-section 3.2.3. In other words, for CEMI, our results mean that only 10% of the gas flow ($K_{rg}<0.1$) takes place in $(1-S_w)=58\%$ of the accessible pore volume, which, according to Kelvin–Laplace's law, is composed of the largest pores ($d^i>2.5$ nm). For CEMV, the pore volume corresponding to 10% of the gas flow is of 28%.

3.3.2. De-saturation and re-saturation phases

Although a strong hysteretic effect is observed for sorption isotherms (S_w vs. *RH*), see Figs. 10 and 11 and also [17], very little information exists on a possible hysteretic phenomenon for gas relative permeability vs. S_w. To be consistent, comparison must be made at the same saturation level S_w, obtained during either drying or imbibition. Figs. 14 and 15 present gas relative permeability K_{rg} vs. S_w during desorption and during the subsequent sorption phase, for CEMI and CEMV concretes, on (a): a linear scale and (b): on a logarithmic scale. The three sorption measurements correspond to the same duration at given *RH* as on the isotherms: for CEMI, 80, 380 and 540 days; for CEMV, 120, 340 and 490 days. Also, fitting results by Van Genuchten-Mualem's model [2,4,5] are presented, see Sub-section 3.3.3 below.

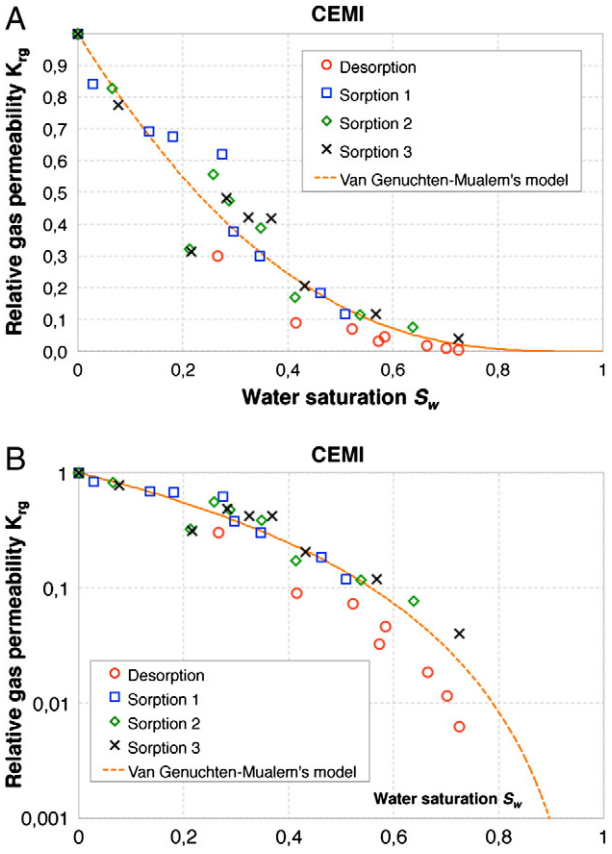

Fig. 14. K_{rg} vs. S_w for CEMI during de-sorption and sorption paths at, respectively, 80, 380, and 540 days; (A): in linear scale; (B): in logarithmic scale.

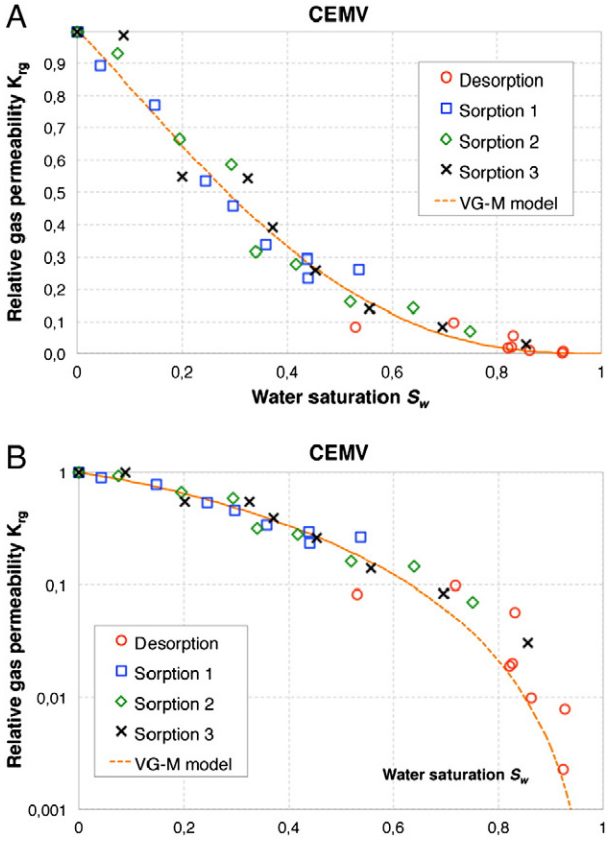

Fig. 15. K_{rg} vs. $S£\%_M$ for CEMV: (1) during de-sorption and sorption paths at, respectively, 120, 340, 490 days; (A): in linear scale; (B): in logarithmic scale.

Experimental data present no ambiguity for CEMV as, both on linear and logarithmic scales, relative permeabilities depend upon saturation only, whatever the saturation path, see Fig. 15. For instance, $S_w = 71\%$ corresponds to $RH = 43\%$ ($P_{cap} = 114$ MPa) during de-sorption and $RH = 92\%$ ($P_{cap} = 11$ MPa) during re-saturation, for similar K_{rg} values of 0.083–0.098. For CEMV concrete, saturation S_w is the sole variable, which controls relative gas permeability. Nevertheless, S_w is not actually a *state* variable, in the thermodynamics sense, as used within the poro-mechanical framework of partially-saturated media.

For CEMI concrete, the analysis, mainly on the logarithmic scale, is not so straightforward. From $S_w = 0$ to 40%, K_{rg} may be considered a sole function of S_w, whereas there are significant differences for $S_w = 40$ to 75%, depending on the sorption/de-sorption path followed. Indeed, when saturation S_w increases above 40%, relative gas permeability, obtained during the re-saturation phase, becomes progressively higher and higher than that measured during de-sorption. At the highest saturation level of 73%, there is an order of magnitude difference between gas relative permeability, either on the sorption or on the de-sorption path. This means that, even if saturation is identical, a hydraulic cut-off remains in de-sorption, which is not present during subsequent re-saturation.

Several interpretations may be proposed (and validated) to explain this observation. First, the complete de-sorption/sorption cycle may have generated micro-cracks, mainly during the drying process. To check this assumption, a complementary test has been performed on the most saturated CEMI sample ($S_w = 73\%$, subjected to $RH = 98\%$), see Table 2. The idea was to measure its gas effective permeability under increasing confining pressure, so that, if present, micro-cracks would close and gas permeability would decrease significantly [23]. Results obtained with four increasing values of confining pressure clearly show that gas effective permeability is divided by two at most (at 20 MPa confinement), see Table 2. This is much lower than the division by 10 (one order of magnitude) observed between the de-sorption and sorption paths at 98%*RH* ($P_{cap} = 2.7$ MPa). Therefore, the presence of micro-cracks is not sufficient to explain the difference in K_{rg} between de-sorption and sorption. Secondly, carbonation, when present, would lead to a decrease in permeability in the vicinity of the sample surface, and to limited micro-cracking due to local swelling [53]. As none of these have been observed here, carbonation may not be invoked to explain the difference in K_{rg} between de-sorption and sorption.

Thirdly, for a part of the observed results, capillary effects may be accounted for. Indeed, capillary pressure P_{cap} described by Kelvin's law (see Eq. (9)) has an influence on, at least, two aspects: 1) conjugated with capillary Laplace's law, P_{cap} is the parameter controlling the pore volume filled with water or not (by providing the smallest drained pore diameter, see Eq. (8)); 2) P_{cap} acts as a pre-stress on the concrete pore network, which affects pore space volume variations and micro-crack closure [54]. Due to these, K_{rg} is expected to depend on both S_w and P_{cap}, i.e. on the sorption/desorption path actually followed. This is the case for CEMI concrete, see Figs. 10 and 14. Each given $S_w > 40\%$ is obtained at a greater *RH* (i.e. smaller P_{cap}) during re-saturation than during desorption. Simultaneously, a given $S_w > 40\%$ corresponds to a greater K_{rg} during re-saturation than during desorption. For instance, $S_w = 52\%$ is obtained in desorption at $RH = 59\%$ ($P_{cap} = 71$ MPa) with $K_{rg}(\text{desorption}) = 0.072$, and during re-saturation $RH = 92$–98% ($P_{cap} = 2.7$–11.3 MPa) with $K_{rg}(\text{re-saturation}) = 0.12$. Also, $S_w = 43\%$ corresponds to $K_{rg}(\text{desorption}) = 6.3 \times 10^{-2}$ at $RH = 43\%$ ($P_{cap} = 114$ MPa), $K_{rg}(\text{re-saturation}) = 0.17$–$0.2$ at $RH = 85$–92% ($P_{cap} = 11$–22 MPa). This means that smaller P_{cap} is related to greater K_{rg}, i.e. smaller capillary pressure tends to facilitate gas passage, possibly by inducing smaller pore volume decrease. The greatest difference (by ca. one order of magnitude) is obtained at $S_w = 72.5\%$, with $K_{rg}(\text{desorption}) = 6.3 \times 10^{-3}$ at $RH = 98\%$, $K_{rg}(\text{resaturation}) = 4.2 \times 10^{-2}$ at $RH = 98\%$.

Further, the complex arrangement of small pore throats and larger capillary pores [18,48,52], which form the whole accessible pore network, may also be at the origin of differing water distribution between sorption and desorption, which implies differing gas transport ability between both path types. In particular, after full de-sorption, water has more difficulty in entering the pore network again due to the existence of small pore throats (bottle neck effect [48]), so that relative gas permeability is smaller during first de-sorption than along the subsequent re-saturation phase. This would require better knowledge of the 3D pore network arrangement, down to very fine nanoscopic pores.

When assuming that the pore network is made of an array of through cylindrical holes of varying diameters d^i, Kelvin–Laplace's law shows that all pores corresponding to $RH < 98.5\%$ are smaller than 50 nm: this is the domain of C–S–H pores [24,40,42], and not of so-called capillary pores. Let us assume that gas transport below 98.5%*RH* occurs within C–S–H porosity: this comes to neglecting bottle neck effects, whereby easy access is not given to large pores, due to pore throat presence, so that these remain water-saturated contrarily to Kelvin–Laplace's law prediction. When considering C–S–H porosity only, Jennings [38] proposes that, when de-saturating C–S–H particles (or globules) from the fully-water saturated state, as is the case here, subsequent re-saturation does not allow water molecules to fill up again all nanoscopic C–S–H particle voids, due to shrinkage irreversibilities at the low C–S–H particle scale. If such phenomena actually occur, at identical saturation level S_w, water would be in greater amount within intra-globular C–S–H gel pores during the first de-sorption phase, rather than during the subsequent sorption phase, hence making water intake more difficult. Moreover, Scrivener et al. [55] recall the significant difference between C–S–H formed in ordinary Portland cement (like CEMI) and those formed in blended cements (such as CEMV): this difference is a morphological one, which is described as a so-called "refinement" and improvement in blended material properties, e.g. smaller gas transport. Chen et al. [32] also recall that C–S–H formed from pozzolanic reaction present smaller (C/S) ratio, so that the amount of water bound to these C–S–H is smaller than in CEMI cement paste. In support to this, thermo-gravimetric analysis (TGA) results in [32] reveal a wider C–S–H stoichiometry for CEMV cement paste than for ordinary cement paste. Due to such morphological features, "coarser" C–S–H present in CEMI concrete would lead to greater shrinkage irreversibilities than "finer" C–S–H, as those present in CEMV. This justifies that a greater difference in K_{rg} is observed after a de-sorption/sorption path for CEMI (than for CEMV). Nevertheless, due to the very low scale involved, no proof exists at this stage that shrinkage irreversibilities, such as described by [38], actually occur in CEMI or CEMV concretes. As Scrivener et al. [55] recall, this is still a research subject.

For CEMI, the difference in gas permeability after a first de-sorption has, however, to be tempered. Fig. 14(b) shows that relative gas permeability has significant values, in the higher range [0.14;1], mainly between $S_w = 0$ and 50%, which are measured mainly during the sorption phase. This means that only 14% of the gas flow (i.e. $K_{rg} < 0.14$) occurs in the higher saturation range (from 50 to 73% S_w). In this higher saturation range, the ratio in relative permeability between de-sorption and sorption paths is, indeed, as low as (1/10), but this represents a very little part (14%) of the total gas flow when the material is at $S_w < 50\%$. As a result, the actual relative gas permeability of CEMI during re-saturation is over-estimated above 50% S_w only, yet with very small values ($K_{rg} < 0.14$). This explains that adequate fitting is achieved with one single parameter values of the

Table 2
Variation of effective gas permeability K_{eff} with confining pressure P_c — example of a CEMI sample successively subjected to 98%*RH*, 60 °C oven-drying, and 98%*RH* again before permeability testing under varying P_c.

P_c (MPa)	5	10	15	20
K_{eff} (10^{-19} m^2)	1.9	1.88	1.27	0.9

Table 3
Fitting parameters for the Van Genuchten–Mualem's model and associated Pearson's correlation coefficient R^2, obtained by the least squares method.

Concrete type/parameter	η	$m = 1-(1/n)$	n	R^2
CEMI	2.65	0.348	1.534	0.935
CEMV	1.14	0.746	3.94	0.977

Van Genuchten–Mualem's statistical model for each concrete, as follows.

3.3.3. Fitting by Van Genuchten–Mualem's model

The conjugated Van Genuchten–Mualem's statistical model [2,4,5] relates relative gas permeability to water saturation level S_w as follows:

$$K_{rg} = (1-S_w)^{\eta}\left(1-S_w{}^{1/m}\right)^{2m} \quad (11)$$

where η is a so-called tortuosity parameter and m is a fitting parameter without actual physical meaning. An assumption is made for m: $m = 1-1/n$ and $n > 1$. η is often taken as 0.5 by default for soils [5], yet it has been reported to vary significantly for concretes [3]. Therefore, both parameters η and m are fitted, using the least squares method, see Table 3. Carlier et al. [3] report that η is all the more so small as the porous medium has a finer texture. Here, CEMI has greater value for η than CEMV, hinting at finer microstructure for the latter. This seems in good agreement with former analysis, see Sub-section 3.2.3.

In order to quantify the fitting adequacy, Pearson's correlation coefficient R^2 is also assessed, see Table 3. It is noted that both fittings present R^2 coefficients higher than 90%, which means adequate correlation of Van Genuchten–Mualem's model for both CEMI and CEMV concretes, despite the small limitations described above (see Sub-section 3.3.2). These parameter values are useful for numerical modelling of gas transport properties of CEMI and CEMV concretes in the partially-saturated state, both for de-sorption and re-saturation.

4. Concluding remarks

This study highlights the considerable effect of the pore microstructure of concrete, as regard sorption/desorption curves and gas relative permeability evolution, after a complete experimental study on two different industrial concrete materials.

Our main results are summarized as follows:

- Total connected porosity ϕ depends significantly on the concrete batch considered, and on the drying temperature (60 or 105 °C). It is of 8.3%+/−0.5 for CEMI concrete and of a greater 10.3%+/−0.7 for CEMV concrete.
- Intrinsic (dry) gas permeability K_{int} is similar for both concretes: its average value is 3.4×10^{-18} m^2 ($+/-0.9\times10^{-18}$ m^2) for CEMI and 3.5×10^{-18} m^2 ($+/-1.1\times10^{-18}$ m^2) for CEMV at a confinement $P_c = 5$ MPa. K_{int} depends on concrete batch, mechanical loading. Correlation between ϕ and K_{int} exists for CEMI, yet not for CEMV.
- In terms of water retention properties, slower mass variation kinetics are recorded for CEMV than for CEMI. During first desorption, CEMV displays greater water retention capacity than CEMI, in direct relation with its greater number of small, nanoscopic, C–S–H pores (2–50 nm). Finally, the total mass loss after 60 °C oven-drying is greater for CEMV than CEMI, in relation with greater porosity ϕ for CEMV.
- The greater number of fine nanoscopic C–S–H pores in CEMV when compared to CEMI is proven by several means: MIP data from [16], analysis of specific surface from the BET theory, and results of stoichiometry models quoted from the literature [14,49].
- Desorption isotherms in this study fit well with previous studies on the same concrete formulations [14,16]. A strong hysteresis in desorption/re-saturation isotherms $S_w(RH)$ is observed for both materials. Together with differences in relative gas permeability $K_{rg}(S_w)$ during desorption/re-saturation of CEMI, this is interpreted as being due to either 1) bottle neck effects within the pore network [48,52], or 2) capillary pressure effects [54], or 3) irreversible shrinkage at the scale of C–S–H layers, obtained after 60 °C drying [38,55]. These interpretations require further investigations, yet these are bound to be difficult if nanoscopic C–S–H pores are involved.
- During first desorption, relative gas permeability vs. S_w is not linear for CEMV, whereas it is linear for CEMI. At given K_{rg}, CEMV contains more water than CEMI, i.e. CEMV contains a greater water amount, which does not participate to gas flow, in relation with its greater number of C–S–H pores.
- For CEMV concrete, relative gas permeability K_{rg} only depends on water saturation level S_w, whichever path it has been achieved through (sorption or de-sorption). For this material, such result is of crucial importance with regard to numerical modelling of gas flow in long term nuclear waste storage structures, as one single relationship describes $K_{rg}(S_w)$, without needing to know whether the material is saturating or de-saturating. In terms of relative gas permeability, CEMI concrete behaves like CEMV up to ca. $S_w = 50\%$, with no hysteretic effect. Above this saturation level, relative gas permeability is higher when obtained on a re-saturation path than on the first desorption path. This difference cannot be explained by the sole occurrence of micro-cracking, as shown with a complementary gas permeability test under increasing confinement. Several interpretations are proposed (see above), which deserve further experimental investigations. Nevertheless, gas flow for $S_w > 50\%$ represents a limited contribution, with $K_{rg} < 0.14$. Due to this, fitting of $K_{rg}(S_w)$ by the Van Genuchten–Mualem's model is achieved convincingly with a *single* set of parameter values per material.

References

[1] Dossier Andra, Référentiel des matériaux d'un stockage de déchets à haute activité et à vie longue, Tome 2: matériaux cimentaires, Document interne Andra n° CRPASCM040015T2_A2005, 2005 (in French).
[2] E. Dana, F. Skoczylas, Experimental study of two-phase flow in three sandstones. II. Capillary pressure curve measurement and relative permeability pore space capillary models, Int. J. Multiphase Flow 28 (2002) 1965–1981.
[3] J.P. Carlier, N. Burlion, Experimental and numerical assessment of the hydrodynamical properties of cementitious materials, Transp. Porous Med. 86 (2011) 87–102.
[4] M.T. Van Genuchten, A closed form equation for predicting the hydraulic conductivity of unsaturated soils, Soil Sci. Soc. Am. J. 44 (1980).
[5] Y. Mualem, New model for predicting hydraulic conductivity of unsaturated porous-media, Water Resour. Res. 12 (3) (1976) 513–522.
[6] J.P. Monlouis-Bonnaire, J. Verdier, B. Perrin, Prediction of the relative permeability to gas flow of cement-based materials, Cem. Concr. Res. 34 (2004) 737–744.
[7] V. Navarro, A. Yustres, L. Cea, M. Candel, R. Juncosa, J. Delgado, Characterization of the water flow through concrete based on parameter estimation from infiltration tests, Cem. Concr. Res. 36 (2006) 1575–1582.
[8] L. Jason, G. Pijaudier-Cabot, S. Ghavamian, A. Huerta, Hydraulic behaviour of a representative structural volume for containment buildings, Nucl. Eng. Des. 237 (2007) 1259–1274.
[9] O. Ippisch, H.-J. Vogel, P. Bastian, Validity limits for the van Genuchten–Mualem model and implications for parameter estimation and numerical simulation, Adv. Water Res. 29 (2006) 1780–1789.
[10] V. Boel, K. Audenaert, G. De Schutter, Modelling of gas permeability in self-compacting concrete, 5th International Essen Workshop — Transport in Concrete, June 11–13 2007.
[11] C. de Sa, F. Benboudjema, M. Thiery, J. Sicard, Analysis of micro-cracking induced by differential drying shrinkage, Cem. Concr. Compos. 30 (2008) 947–956.
[12] I. Yurtdas, Couplage comportement mécanique et dessiccation des matériaux à matrice cimentaire: étude expérimentale sur mortier, thèse de doctorat de l' Université des Sciences et Technologies de Lille, 2003 (in French).
[13] S. M'Jahad, W. Chen, C.A. Davy, F. Skoczylas, X. Bourbon, Gas relative permeability of damaged concrete: effect of hydrostatic stress and water saturation rate, 13th International Conference on the Chemistry of Cement (XIII ICCC), Madrid, July 2011.
[14] H. Ranaivomanana, J. Verdier, A. Sellier, X. Bourbon, Toward a better comprehension and modeling of hysteresis cycles in the water sorption–desorption process for cement based materials, Cem. Concr. Res. 41 (2011) 817–827.

[15] S. Poyet, Experimental investigation of the effect of temperature on the first desorption isotherm of concrete, Cem. Concr. Res. 39 (11) (2009) 1060–1067.
[16] F.N.G. Brue, C.A. Davy, F. Skoczylas, N. Burlion, X. Bourbon, Effect of temperature on the water retention properties of two high performance concretes, Cem. Concr. Res. 42 (2) (2012) 384–396.
[17] V. Baroghel-Bouny, Water vapour sorption experiments on hardened cementitious materials Part I: essential tool for analysis of hygral behaviour and its relation to pore structure, Cem. Concr. Res. 37 (2007) 414–437.
[18] R.M. Espinosa, L. Franke, Influence of the age and drying process on pore structure and sorption isotherms of hardened cement paste, Cem. Concr. Res. 36 (2006) 1969–1984.
[19] Andra, Choix des formulations de référence: ciment CPA-CEM I, Caractéristiques mécaniques et de durabilité, Document interne Andra n° C RP 0 CTP 01-002/A, 2001 (in French).
[20] Andra, Choix des formulations de bétons de référence, Document interne Andra n° C RP 0 LER 01-004/A, 2001 (in French).
[21] J. Verdier, M. Carcassès, J.-P. Ollivier, Modelling of a gas flow measurement — application to nuclear waste containment vessels, Cem. Concr. Res. 32 (2002) 1331–1340.
[22] C. Gallé, Effect of drying on cement-based materials pore structure as identified by mercury intrusion porosimetry a comparative study between oven-, vacuum-, and freeze-drying, Cem. Concr. Res. 31 (2001) 1467–1477.
[23] X.-T. Chen, C.A. Davy, J.F. Shao, F. Skoczylas, Experimental and micro-mechanical analysis of the mechanical and transport properties of mortar containing heat-induced micro-cracks, Cem. Concr. Compos. 32 (2010) 678–685.
[24] Z. Sun, G.W. Scherer, Pore size and shape in mortar by thermoporometry, Cem. Concr. Res. 40 (2010) 740–751.
[25] F.-A. Sarott, M.H. Bradbury, P. Pandolfo, P. Spieler, Diffusion and adsorption studies on hardened cement paste and the effect of carbonation on diffusion rates, Cem. Concr. Res. 22 (2–3) (1992) 439–444.
[26] V. Baroghel-Bouny, M. Mainguy, T. Lassabatère, O. Coussy, Characterization and identification of equilibrium and transfer moisture properties for ordinary and high-performance cementitious materials, Cem. Concr. Res. 29 (1999) 1225–1238.
[27] E. Dana, F. Skoczylas, Experimental study of two-phase flow in three sandstones. I. Measuring relative permeabilities during two-phase steady-state experiments, Int. J. Multiphase Flow 28 (2002) 1719–1736.
[28] A. Abbas, M. Carcasses, J.-P. Ollivier, Gas permeability of concrete in relation to its degree of saturation, Mater. Struct. 32 (1999) 3–8.
[29] F. Skoczylas, J.P. Henry, A study of the intrinsic permeability of granite to gas, Int. J. Rock Mech. Min. Sci. & Geomech. Abstr. 32 (2) (1995) 171–179.
[30] I.J. Klinkenberg, The permeability of porous media to liquids and gases, API Drilling and Production Practices, 1941, pp. 200–213.
[31] Y. Benachour, C.A. Davy, F. Skoczylas, H. Houari, Effect of a high calcite filler addition upon microstructural, mechanical, shrinkage and transport properties of a mortar, Cem. Concr. Res. 38 (2008) 727–736.
[32] X.-T. Chen, Th. Rougelot, C.A. Davy, W. Chen, F. Agostini, F. Skoczylas, X. Bourbon, Experimental evidence of a moisture clog effect in cement-based materials under temperature, Cem. Concr. Res. 39 (2009) 1139–1148.
[33] N. Burlion, F. Skoczylas, T. Dubois, Induced anisotropic permeability due to drying of concrete, Cem. Concr. Res. 33 (2003) 679–687.
[34] F. Skoczylas, O. Coussy, Z. Lafhaj, Sur la fiabilité des mesures des perméabilités hétérogènes par injection de gaz. Micro-pulse tests, Rev. Fr. de Génie Civ. 7 (2003) 451–469.
[35] H. Loosveldt, Z. Lafhaj, F. Skoczylas, Experimental study of gas and liquid permeability, Cem. Concr. Res. 32 (2002) 1357–1363.
[36] P. Van den Heede, E. Gruyaert, N. De Belie, Transport properties of high-volume fly ash concrete: capillary water sorption, water sorption under vacuum and gas permeability, Cem. Concr. Res. 32 (2010) 749–756.
[37] Z. Lafhaj, M. Goueygou, A. Djerbi, M. Kaczmarek, Correlation between porosity, permeability and ultrasonic parameters of mortar with variable water/cement ratio and water content, Cem. Concr. Res. 36 (4) (2006) 625–633.
[38] H.M. Jennings, Refinements to colloid model of C–S–H in cement: CM-II, Cem. Concr. Res. 38 (2008) 275–289.
[39] W.V. Kayser, Temperature dependence of the surface tension water in contact with its saturated vapour, J. Colloid Interface Sci. 56 (1976) 622–627.
[40] P.J. McDonald, V. Rodin, A. Valori, Characterisation of intra- and inter-C–S–H gel pore water in white cement based on an analysis of NMR signal amplitudes as a function of water content, Cem. Concr. Res. 40 (12) (2010) 1656–1663.
[41] J. Baron, R. Sauterey, Le béton hydraulique, Presses de l' Ecole Nationale des Ponts et Chaussées, 1982 560 pp. (in French).
[42] S. Mindess, J.F. Young, D. Darwin, Concrete, 2nd Edition Prentice Hall, Englewood Cliffs, NJ, 2002.
[43] A. Lobet, Influence des paramètres de composition des matériaux cimentaires sur les propriétés de transfert, thèse de doctorat de l'INSA de Toulouse, 2003 (in French).
[44] C.A. Davy, F. Skoczylas, W. Chen, J. Liu, F. Brue, S. M' Jahad, Experimental identification of two phase flow parameters for CEMI and CEMV-based concretes, (in English), Andra GL Transfert de gaz Annual meeting, Châtenay-Malabry, France, January 25th 2012.
[45] J.F. Daian, Equilibre et transferts en milieux poreux, première partie: Etats d'équilibre, 2010 188 pp. (in French).
[46] S. Brunauer, P.H. Emmett, E. Teller, Adsorption of gases in multimolecular layers, J. Am. Chem. Soc. 60 (2) (1938) 309–319.
[47] J.A. Odutola, T.R. Dyke, Partially deuterated water dimmers: microwave spectra and structure, J. Chem. Phys. 72 (1980) 5062–5070.
[48] S. Diamond, Mercury porosimetry: an inappropriate method for the measurement of pore size distributions in cement-based materials, Cem. Concr. Res. 30 (2000) 1517–1525.
[49] E. Drouet, Impact de la température sur la carbonatation des matériaux cimentaires – prise en compte des transferts hydriques. Thèse de Doctorat (PhD Thesis, in French), Ecole Normale Supérieure de Cachan, France, 2010.
[50] C. Perlot, J. Verdier, M. Carcassès, Influence of cement type on transport properties and chemical degradation: application to nuclear waste storage, Mat. Struct. 39 (2006) 511–523.
[51] S. Kourounis, S. Tsivilis, P.E. Tsakiridis, G.D. Papadimitriou, Z. Tsibouki, Properties and hydration of blended cements with steelmaking slag, Cem. Concr. Res. 37 (2007) 815–822.
[52] T. Ishida, K. Maekawa, T. Kishi, Enhanced modeling of moisture equilibrium and transport in cementitious materials under arbitrary temperature and relative humidity history, Cem. Concr. Res. 37 (2007) 565–578.
[53] J.J. Thomas, J.H. Seieh, H.M. Jennings, Effect of carbonation on the nitrogen BET surface area of hardened Portland cement paste, Adv. Cem. Based Mater. 3 (1996) 76–80.
[54] F. Skoczylas, N. Burlion, I. Yurtdas, About drying effects and poro-mechanical behaviour of mortars, Cem. Concr. Compos. 29 (5) (2007) 383–390.
[55] K.L. Scrivener, A. Nonat / Cem. Concr. Res. 41 (2011) 651–665.